Modeling of Bulk Delivery Systems for Supplying Electronic Specialty Gases at High Flow Rates

M. Usman Ghani[1], Richard Udischas[1], Valerie Nille[2] and Derong Zhou[3]

[1] American Air Liquide, Chicago Research Center, 5230 S. East Ave, Countryside, IL 60525
[2] Air Liquide Electronics Materials, 1 rue Georges Claude, Chalon-sur-Saone, France 71106
[3] Air Liquide America L.P., 19 Steel Road West, Morrisville, PA 19067

Abstract

More and more manufacturing processes for semiconductor, fiber optics, and flat panel display demand a consistent supply of electronic specialty gases (ESGs) at high flow rates. Bulk delivery systems have been developed to meet such a demand with the advantages of reduction in potential contamination, improved safety and handling and lower costs. A bulk delivery system typically uses ton containers and ISO containers to source ESGs for a longer period of time while maintaining a required delivery pressure.

This paper presents a model that has been developed to predict the temperature and pressure in a bulk delivery container as a function of gas withdrawal rate under dynamic conditions. The model is based upon a previous model developed at American Air Liquide for ESG cylinders and vapor pressure correlations for various ESGs. The mathematical formulation includes heat transfer due to the vaporization of a liquefied ESG as well as heat transfer from ambient to the container and then to ESG. The model assumes a uniform liquid temperature but the vapor phase and container wall temperatures are allowed to vary with position but in one dimension. The method of lines is used to solve the governing equations. The resulting system of ODEs is solved using the LSODE solver.

The model predictions are compared with a lab-scale "mini ton vessel" with C_3F_8 and a commercial ton vessel with three different ESGs, namely Chlorine (Cl_2), Hydrogen Bromide (HBr), and Boron Trichloride (BCl_3). The model predictions are in good agreement with experimental results of these ESGs at actual operating conditions. The model allows us to propose a proper design for a bulk delivery system for any given ESG by considering the size of the source container and all downstream components in addition to the flow and pressure requirements.

Introduction

The demand for ESGs at high flow rates is on the rise due to increased production capacities of semiconductors, fiber optics, and flat panel displays. This demand is usually met using bulk delivery systems. A typical bulk delivery system uses ton containers (about 450 liters or 820 liters capacity) or ISO containers (about 24,000 liters capacity) to source ESGs for a longer period of time while maintaining a required delivery pressure. The bulk delivery systems offer a number of advantages, over a cylinder bundle, as follows:

1. Capability to deliver much higher flow rates of gas for longer periods of time.

2. Reduction in potential contamination due to less frequent switchovers.
3. Improved safety and handling due to less operator intervention.
4. Lower costs due to bulk supply and savings resulting from lower transportation costs.

A model has been developed to predict pressure in a bulk delivery container as a function of gas withdrawal rate. A bulk delivery system would be supplying an ESG to a number of tools. The gas withdrawal is, therefore, imposed (i.e., provided as an input) in this model according to the recipe of the manufacturing process. The ESG is usually needed at a certain pressure at the point of use (POU). Therefore, the prediction of pressure in the container is important to ensure that the supply pressure requirement could be met. If at the desired gas usage pattern, large quantity of ESG exists when the supply pressure drops below the required value, heating of the vessel may be necessary to maintain supply pressure. The model provides an option to include heating of the container. In this paper, however, the focus is on bulk delivery systems without an external heat source. This model has been incorporated in an Air Liquide Proprietary software *v*INTAL, which is a user-friendly windows based package. The software, *v*INTAL, includes physical properties for a large number of ESGs to predict pressure in the delivery system given the usage pattern. It is also noted that the bulk delivery systems could be used to deliver either vapor product or liquid product as shown in Figure 1. The model presented in this paper deals only with the delivery of the vapor phase product. However, the model could be easily adapted for delivery of liquid phase product.

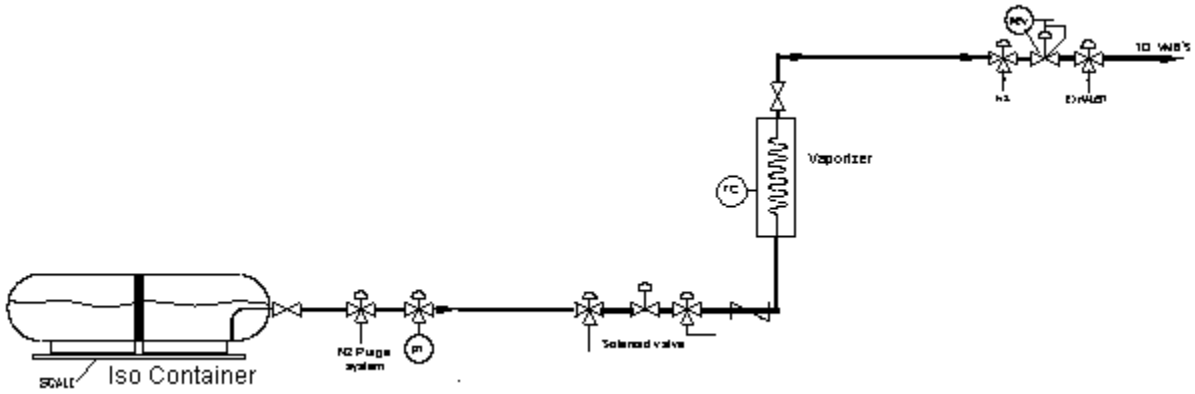

Figure 1. Liquid delivery from a bulk container.

Model Basics

The model, presented in this paper, is based upon a previous model (Jurcik, 1996) developed at American Air Liquide for ESG cylinders and pressure drop data correlations for various ESGs. The vessel geometry as used in this model is simplified. A typical bulk delivery vessel is a horizontal cylinder with ellipsoidal heads as shown in Figure 2a. In our model, we will consider a horizontal cylinder with flat heads as shown in Figure 2b. The length of the vessel is accordingly adjusted to account for the modified geometry to provide the same internal volume.

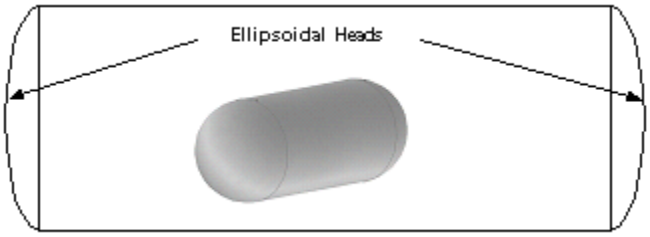

Figure 2a. Typical horizontal bulk delivery vessel

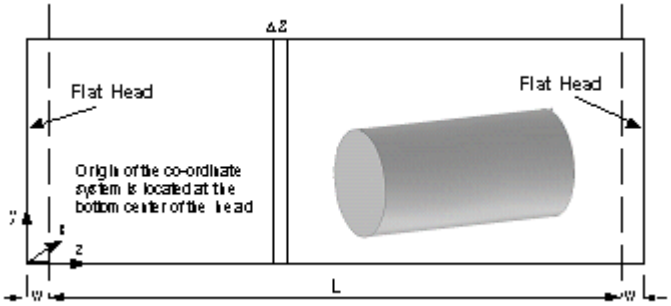

Figure 2b. Geometry of horizontal bulk delivery vessel as used in the model.

The model takes into account heat transfer due to the vaporization of a liquefied ESG as well as heat transfer from ambient to the container and then to ESG. The basic assumptions made in the formulation of this model are as follows:

1. The liquid temperature is considered uniform. Thus, there are no buoyancy driven currents, i.e., liquid is stagnant.
2. The cylinder is modeled as an infinite cylinder. Thus, temperature does not depend on the axial (i.e., longitudinal) position as shown in Figure 2b.
3. The vapor temperature field is stratified, i.e., varies only in the vertical direction, as shown in Figure 3.
4. The temperature drop across the vessel walls is negligible, i.e., there is no temperature gradient in the radial direction.
5. Conduction is allowed in the vessel walls but only azimuthally.
6. The amount of vapor withdrawn is compensated by the same amount of liquefied ESG vaporizing into the headspace.
7. Heat transfer through the vessel heads is ignored.
8. Vessel is initially in thermal equilibrium.

Figure 3 also shows various heat fluxes considered in the formulation of the model.

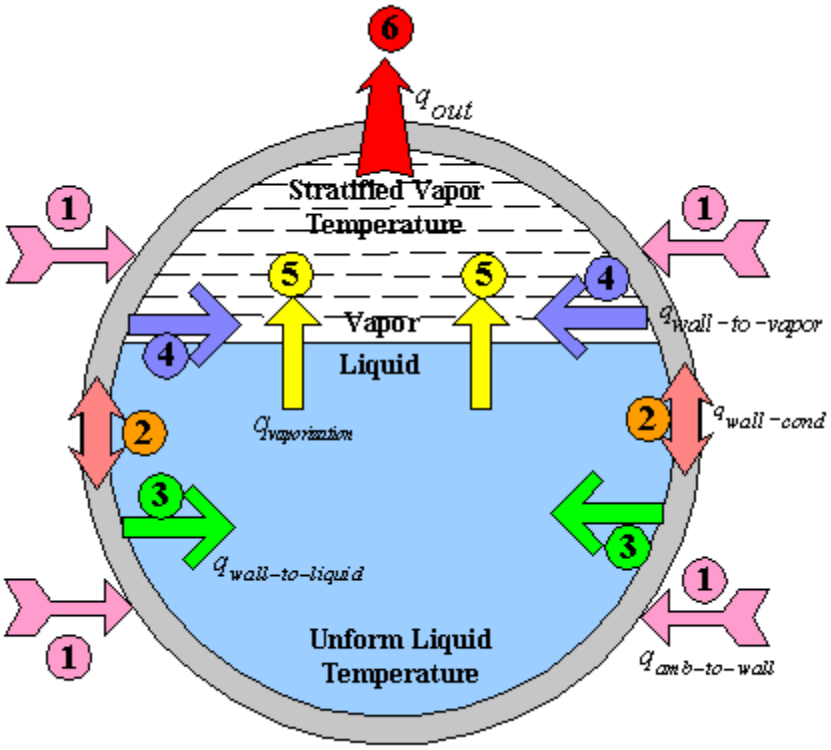

Figure 3. Heat transfer processes as implemented in the model for a slice of thickness Δz.

An additional cylindrical coordinate system (r, θ, z) is also defined at the center of the slice with its axial direction aligned with the axial (z) direction of the Cartesian coordinate system.

Governing Equations

The model is based upon the unsteady mass and energy balances. The differential equations describing these balances are as shown below. The corresponding initial and boundary conditions are also shown.

1. Mass balance:

$$\frac{dm_l(t)}{dt} = -\dot{m}(t) \tag{1}$$

with the initial condition

$$m_l(0) = m_{l,0} \tag{1a}$$

2. Liquid energy balance:

The liquid energy balance is based upon the first law of thermodynamics for an open system and is given by the following expression:

$$m_l(t)\frac{d\hat{U}_l(t)}{dt} = \dot{m}(t)\left[\hat{H}_g(T_{g,top}(t) - \hat{U}_l(t)\right] + 2R_l L\int_0^{\theta_l(t)} h_{w2l}\left[T_w(t,\theta') - T_l(t)\right]d\theta' \tag{2}$$

with the initial condition

$$\hat{U}_l(0) = \hat{U}_l(T_{l,0}) \tag{2a}$$

3. Energy balance on the vessel wall adjacent to liquid:

$$(R_o^2 - R_i^2)\rho_c c_c \frac{\partial T_{wl}(t,\theta)}{\partial t} = R_o h_{a2w}\left[(T_\infty - T_{wl}(t,\theta)\right] - R_i h_{w2l}\left[T_{wl}(t,\theta) - T_l(t)\right] + \left(\frac{R_o - R_i}{R_m}\right)k_c \frac{\partial^2 T_{wl}(t,\theta)}{\partial\theta^2} \tag{3}$$

with the initial and boundary conditions

$$T_{wl}(0,\theta) = T_{wl,0} \qquad -\theta_l \le \theta \le \theta_l \tag{3a}$$

$$\frac{\partial T_{wl}(t,0)}{\partial\theta} = 0 \qquad t \ge 0 \tag{3b}$$

$$T_{wl}(t,\theta_l) = T_{wv}(t,\theta_l) \qquad t \ge 0 \tag{3c}$$

4. Energy balance on the vessel wall adjacent to vapor:

$$(R_o^2 - R_i^2)\rho_c c_c \frac{\partial T_{wv}(t,\theta)}{\partial t} = R_o h_{a2w}\left[(T_\infty - T_{wv}(t,\theta)\right] - R_i h_{w2v}\left[T_{wv}(t,\theta) - T_v(t,y)\right] + \left(\frac{R_o - R_i}{R_m}\right)k_c \frac{\partial^2 T_{wv}(t,\theta)}{\partial\theta^2} \tag{4}$$

with the initial and boundary conditions

$$T_{wv}(0,\theta) = T_{wv,0} \qquad -\theta_l \le \theta \le \pi \text{ and } \theta_l \le \theta \le \pi \tag{4a}$$

$$\frac{\partial T_{wv}(t,\pi)}{\partial\theta} = 0 \qquad t \ge 0 \tag{4b}$$

$$T_{wv}(t,\theta_l) = T_{wl}(t,\theta_l) \qquad t \ge 0 \tag{4c}$$

5. Vapor phase Energy balance:

For the vapor phase energy balance, we consider an element, shown shaded in Figure 4, in the vapor region of the vessel.

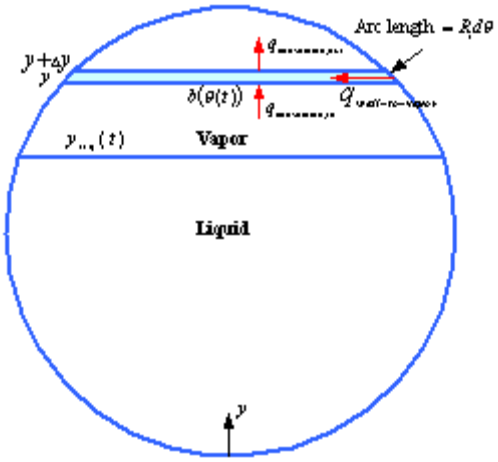

Figure 4. Vapor phase energy balance for the volume element shown.

The energy balance for this element yields:

$$b(y)\rho_g c_p \frac{\partial T_v(t,y)}{\partial t} = 2h_{w2v}\left[T_{wv}(t,\theta) - T_v(t,y)\right] - b(y)V_y \rho_g c_p \frac{\partial T_v(t,y)}{\partial y} \tag{5}$$

with initial and boundary conditions:

$$T_v(0,y_0) = T_{v,0} \qquad 0 \le y \le 2R_i \tag{5a}$$

$$T_v\left(t, y_{liq}(t)\right) = T_{liq}(t) \qquad t \ge 0 \tag{5b}$$

Solution Technique

The governing differential equations are disretized and solved using the Method of Lines (Mageroy, 1997). As the vessel wall temperature and vapor temperature varies, we define N nodes within the vapor phase inside the vessel and along the vessel wall adjacent both to the liquid and vapor, as shown in Figure 5. The resulting discretized equations are presented next.

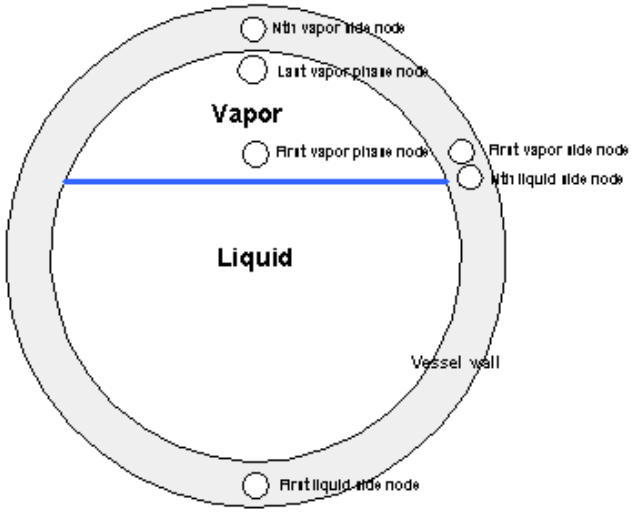

Figure 5. Node locations as used in the discretization of the governing equations.

Vessel wall temperature adjacent to the liquid:

At the first boundary node:

$$(R_o^2 - R_i^2)\rho_c c_c \frac{\partial T_{wl}(t,1)}{\partial t} = R_o h_{a2w}\left[(T_\infty - T_{wl}(t,1)\right] - R_i h_{w2l}\left[T_{wl}(t,1) - T_{liq}(t)\right] + 2\left(\frac{R_o - R_i}{R_m}\right)k_c\left[\frac{T_{wl}(t,2) - T_{wl}(t,1)}{(\Delta\theta)^2}\right] \quad (6a)$$

At the internal nodes:

$$(R_o^2 - R_i^2)\rho_c c_c \frac{\partial T_{wl}(t,i)}{\partial t} = R_o h_{a2w}\left[(T_\infty - T_{wl}(t,i)\right] - R_i h_{w2l}\left[T_{wl}(t,i) - T_{liq}(t)\right] + \left(\frac{R_o - R_i}{R_m}\right)k_c\left[\frac{T_{wl}(t,i+1) - 2T_{wl}(t,i) + T_{wl}(t,i-1)}{(\Delta\theta)^2}\right] \quad (6b)$$

At the last boundary node:

$$(R_o^2 - R_i^2)\rho_c c_c \frac{\partial T_{wl}(t,N)}{\partial t} = R_o h_{a2w}\left[(T_\infty - T_{wl}(t,N)\right] - R_i h_{w2l}\left[T_{wl}(t,N) - T_{liq}(t)\right] + \left(\frac{R_o - R_i}{R_m}\right)k_c\left[\frac{T_{wv}(t,1) - 2T_{wl}(t,N) + T_{wl}(t,N-1)}{(\Delta\theta)^2}\right] \quad (6c)$$

Vessel wall temperature adjacent to the vapor:

At the first boundary node:

$$(R_o^2 - R_i^2)\rho_c c_c \frac{\partial T_{wv}(t,1)}{\partial t} = R_o h_{a2w}\left[(T_\infty - T_{wv}(t,1)\right] - R_i h_{w2v}\left[T_{wv}(t,1) - T_v(t,1)\right] + \left(\frac{R_o - R_i}{R_m}\right)k_c\left[\frac{T_{wv}(t,2) - 2T_{wv}(t,1) + T_{wl}(t,N)}{(\Delta\theta)^2}\right] \quad (7a)$$

At the internal nodes:

$$(R_o^2 - R_i^2)\rho_c c_c \frac{\partial T_{wv}(t,i)}{\partial t} = R_o h_{a2w}\left[(T_\infty - T_{wv}(t,i)\right] - R_i h_{w2v}\left[T_{wv}(t,i) - T_v(t,i)\right] + \left(\frac{R_o - R_i}{R_m}\right)k_c\left[\frac{T_{wv}(t,i+1) - 2T_{wv}(t,i) + T_{wl}(t,i-1)}{(\Delta\theta)^2}\right] \quad (7b)$$

At the last boundary node:

$$(R_o^2 - R_i^2)\rho_c c_c \frac{\partial T_{wv}(t,N)}{\partial t} = R_o h_{a2w}\left[(T_\infty - T_{wv}(t,N)\right]$$
$$-R_i h_{w2v}\left[T_{wv}(t,N) - T_v(t,N)\right] + 2\left(\frac{R_o - R_i}{R_m}\right)k_c\left[\frac{T_{wv}(t,N-1) - T_{wv}(t,N)}{(\Delta\theta)^2}\right] \quad (7c)$$

Vapor phase temperature:

At the first boundary node:

$$b_1\rho_{g,i}c_{p_{g,i}}\frac{\partial T_v(t,1)}{\partial t} = 2h_{w2v}\left[T_{wv}(t,1) - T_v(t,1)\right] - b_1 V_1\rho_{g,i}c_{p_{g,i}}\left[\frac{T_v(t,2) - T_{liq}(t)}{2\Delta y}\right] \quad (8a)$$

At the internal nodes:

$$b_i\rho_g c_{p_g}\frac{\partial T_v(t,i)}{\partial t} = 2h_{w2v}\left[T_{wv}(t,i) - T_v(t,i)\right] - b_i V_i\rho_{g,i}c_{p_{g,i}}\left[\frac{T_v(t,i+1) - T_v(t,i-1)}{2\Delta y}\right] \quad (8b)$$

At the last boundary node:

$$b_N\rho_{g,N}c_{p_{g,N}}\frac{\partial T_v(t,N)}{\partial t} = 2h_{w2v}\left[T_{wv}(t,N) - T_v(t,N)\right] - b_i V_N\rho_{g,i}c_{p_{g,i}}\left[\frac{T_{wv}(t,N) - T_v(t,N-1)}{2\Delta y}\right] \quad (8c)$$

In the above expressions b_i are evaluated at the midpoint of the element i.e., at $y_{node} + \frac{1}{2}\Delta y$.

Solution Procedure

The above discretization results in a system of ordinary differential equations (ODEs) comprising of 3N+2 equations. All these differential equations are converted to the form $y_i' = f\left(y_i, T, ...\right)$. The system of differential equations is solved using the LSODE (Lawrence Livermore Ordinary Differential Equations) Solver. Details of this package are provided by Hindmarsh (1983). The initial state of the bulk delivery system is used to calculate the internal energy of the liquid. The initial height of the liquid ESG in the vessel is also determined by the initial mass of ESG, initial temperature and distribution of the mass between the liquid and vapor phases. The physical properties of the vessel material are considered temperature independent i.e., constant, whereas the physical properties for the ESGs are taken to be temperature dependent. The heat transfer coefficients are calculated using the correlation for forced convection, found in standard engineering heat transfer textbooks (Holman, 1986), using the physical properties that are updated at each time step. A constant value of 5 $\left(\frac{W}{m^2 \bullet s}\right)$ is used for the external (from ambient to vessel) heat transfer coefficient for the ton vessel. For the "mini ton-vessel," a value of 10 $\left(\frac{W}{m^2 \bullet s}\right)$ is used. The heat transfer coefficient from wall to liquid is modified to account for the enhanced heat transfer due to rapid vaporization and associated vigorous boiling. The expression used for this modification is:

$$h_{\text{int}} = A\exp\left(-\frac{(y - y_{\text{int}})}{B}\right) \tag{9}$$

where A and B are constants. The constant A and B are fixed at the same values for all available ESGs in the model.

Once the liquid internal energy is updated, the liquid temperature, at each time step, is then solved using the Newton Raphson method. The pressure is finally determined by using the vapor pressure correlation.

Experimental

Experiments were conducted at our Chicago Research Center facility using a so-called "mini ton-vessel." The mini ton-vessel is a small horizontal cylinder with 2.3 liters internal volume. Experiments were conducted with C_3F_8. The gas withdrawal was regulated with a mass flow controller that was calibrated before the experiment. Three thermocouples were attached to the vessel wall to measure the wall temperatures.

Experiments were also conducted at our Morrisville facility using a commercial ton-vessel having an internal volume of 820 liters. Three ESGs namely BCl_3, HBr and Cl_2 were used for these experiments. A series of seventeen experiments were conducted over a period of a few days, using Cl_2, from a full to nearly empty container at various gas withdrawal rates. A single experiment was run using HBr. The vessel was placed upon a platform, as shown in Figure 6, fitted with a scale to monitor the mass of the vessel. Temperature readings were also measured along the vessel wall. In all experiments, pressure was monitored upstream of the supply valve located on the vessel.

Figure 6. Experimental setup for the bulk delivery system.

Results

This section presents the model predictions and compares the results with the experimental data. The mass flow rate, which is obtained from the experimental data for the mass, is converted to volumetric flow rate in standard liters per minute (*slpm*). The volumetric flow rate is then used as the vapor product withdrawal rate from the vessel. Figure 7 shows typical results that are obtained with the model simulations. In a typical operation, flow would be on for sometime and off for sometime. In the simulation results presented in Figure 7, flow is hypothetically assumed to be on for thirty minutes at 400 *slpm*, then for fifteen minutes with a flow rate of 200 *slpm*, which is followed by a pulse of 300 *slpm*. This cycle is then repeated. However, complex usage patterns of actual manufacturing processes can be easily simulated in our model.

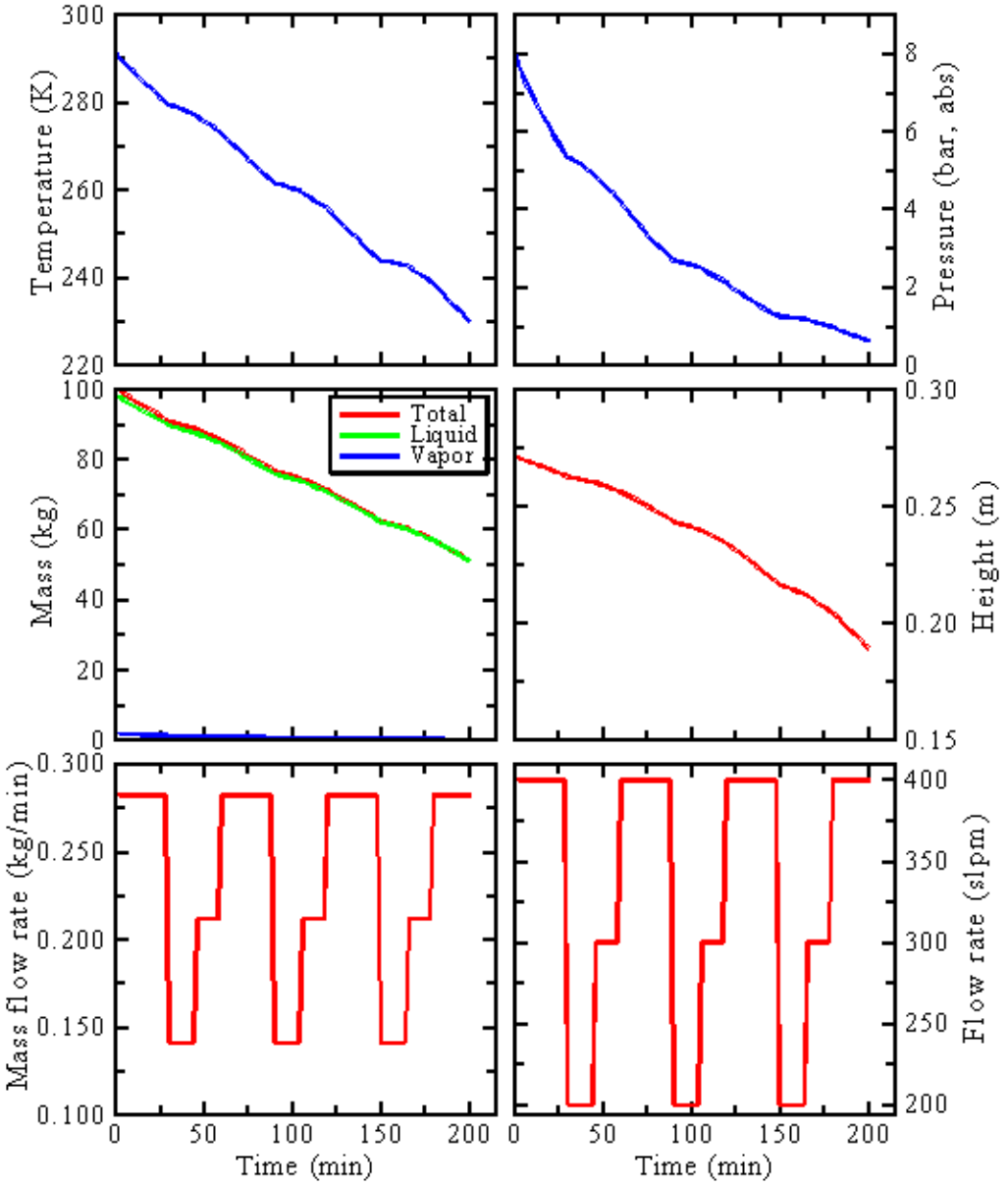

Figure 7. Model prediction for a hypothetical usage pattern from a 450 liters bulk delivery vessel.

Figure 8 shows that the model results for C_3F_8, a medium pressure gas, at a flow rate of 2.75 *slpm* from the "mini ton-vessel." The liquid temperature is computed from the measured pressure using the vapor pressure correlation. The model predictions are in good agreement with the experimental data. Figure 8 also shows the change in liquid height. In contrast with a cylinder, the change in liquid height is non-linear as ESG is withdrawn from the vessel. Figures 9 and 10 show the results for BCl_3 (a low pressure gas) and HBr (a high pressure gas), respectively, in a commercial ton-vessel. These results are also in reasonable agreement with the experimental observations.

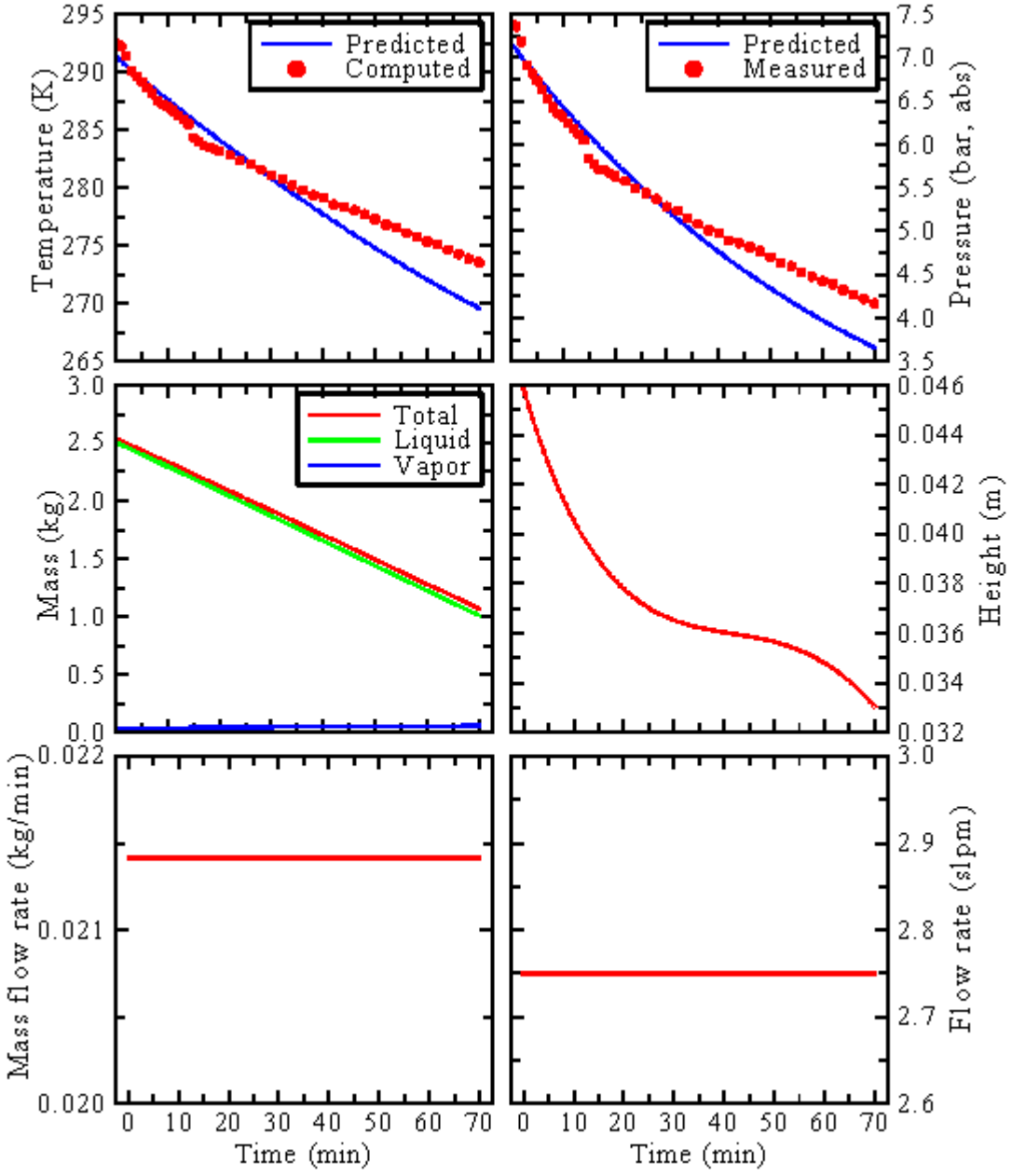

Figure 8. Model prediction for C_3F_8 withdrawn from a "mini ton-vessel" and comparison with the experimental data for pressure and liquid temperature.

Figures 11-13 show the model predictions for Cl_2 in a commercial ton vessel with three different initial charges. In all these cases, the model predictions are in reasonable agreement with the experimental results. The experiments with a full Cl_2 ton-vessel were conducted in seventeen separate runs over a period of three weeks. It is, however, noted that in these runs, the lapse time between some consecutive runs was not sufficient to allow the liquid to equilibrate with the surrounding. Thus, the initial temperature for the liquid mass was adjusted to account for the thermal non-equilibrium state of the system. Work is in progress to analyze this effect and will be reported as it becomes available. It is also pointed out that a better understanding of heat transfer between the vessel and the liquid product is essential to improve the model predictions and to eliminate the adjustable parameters needed for correction of the heat transfer coefficient due to vigorous boiling associated with such withdrawals. This aspect is also focus of current work, which is still in progress.

Conclusions

A computational model has been developed to model the pressure evolution behavior of a bulk delivery system supplying an ESG at high flow rates. Comparisons between the model predictions and experimental data for different gases were presented. These comparisons show a good agreement between the model prediction and experimental data. To account for the vigorous boiling due to high flow rate withdrawal from the vessel, the heat transfer coefficient is modified. Work is in progress to better understand the heat transfer behavior under these conditions.

Acknowledgments

The authors would like to thank Dr. Benjamin Jurcik, of Air Liquide America, for helpful discussion during the course of this work. The authors also wish to thank Mr. Marc Dequesnes, of American Air Liquide, for reviewing the manuscript and making helpful suggestions.

Nomenclature

A	Constant
b	Width, m
B	Constant
c	Heat capacity, $J/(kg \cdot K)$
h	Heat transfer coefficient, $J/(kg \cdot m^2 \cdot K)$
H	Enthalpy, $J/(kg)$
i	Node index
k	Thermal conductivity, $J/(kg \cdot m \cdot K)$
L	Effective length of vessel, m
m	Mass, kg

N	Number of nodes
R	Radius, m
t	Time, s
T	Temperature, K
U	Internal Energy, J/kg
V	Velocity, m/s
y	Liquid height, m
y	Cartesian coordinate, m
Greek	
ρ	Density, kg/m^3
θ	Azimuthal co-ordinate, radian
Subscripts	
$a2w$	External, ambient to wall
0	Initial
g	Gas
i	Inside
∞	Ambient
int	Interface
l	Liquid
liq	Liquid
m	Mean
o	Outside
v	Vapor
wl	Wall, liquid side
wv	Wall, vapor side
$w2l$	Inside, wall to liquid
$w2v$	Inside, wall to vapor

References

Hindmarsh, A. C., "ODEPACK, A Systemized collection of ODE Solvers," in Scientific Computing, (R. S. Stepleman, editor), Vol. 1, p. 55, IMACS Transactions on Scientific Computation, North Holland, Amsterdam, (1983).

Holman, J. P., "Heat Transfer," Sixth Edition, McGraw-Hill Book Company, New York, (1986).

Jurcik, Benjamin, "A Model for Heat Transfer to a cylinder Containing a Gas Stored Under its Own Vapor Pressure," Internal Report, American Air Liquide, Chicago Research Center, (1996).

Mageroy, Einar, "Numerical Integration of Systems Arising from the Method of Lines," Department of Mathematical Sciences, The Norwegian University of Science and Technology, (1997).

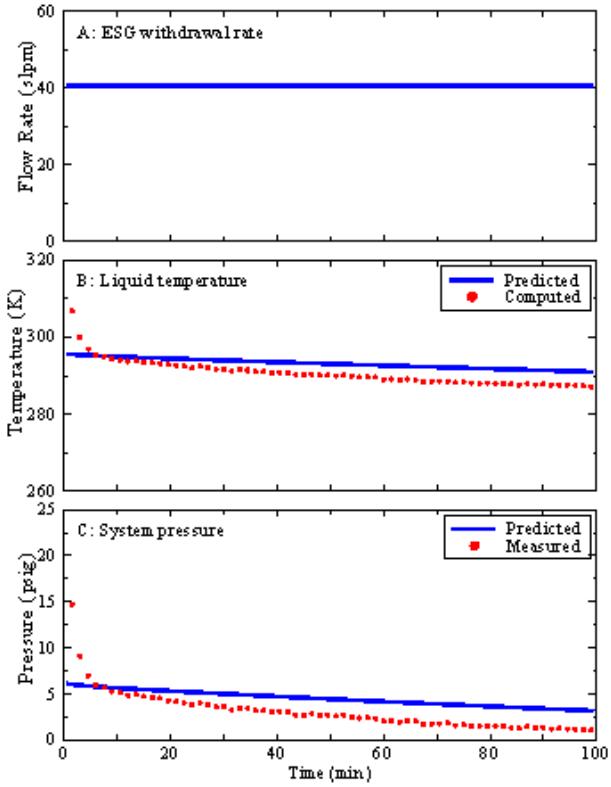

Figure 9. Comparison of model predictions with the experimental data for BCl_3.

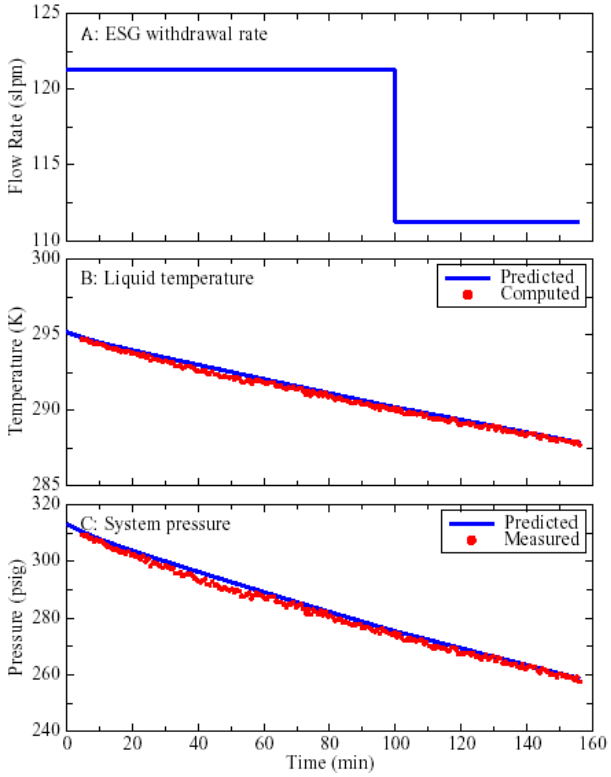

Figure 10. Comparison of model predictions with the experimental data for HBr.

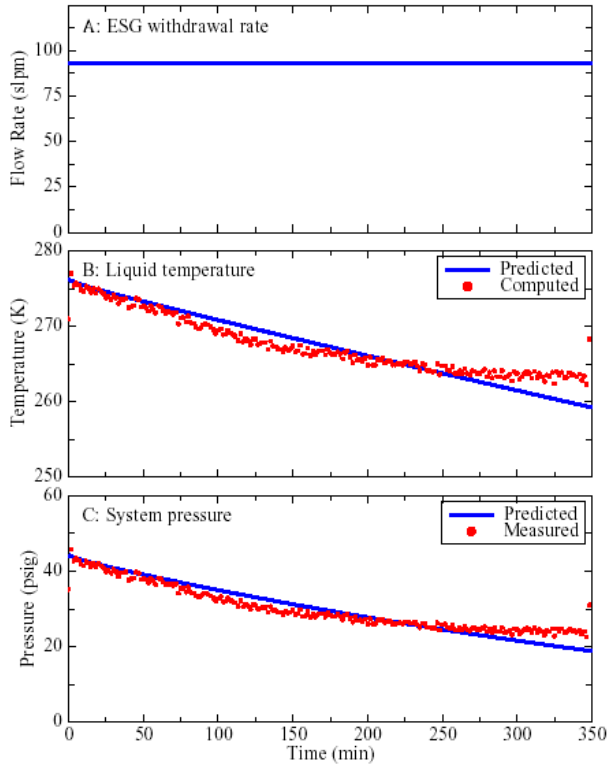

Figure 11. Comparison of model predictions with the experimental data for Cl_2 from a nearly full ton vessel with an initial charge of 800 kg.

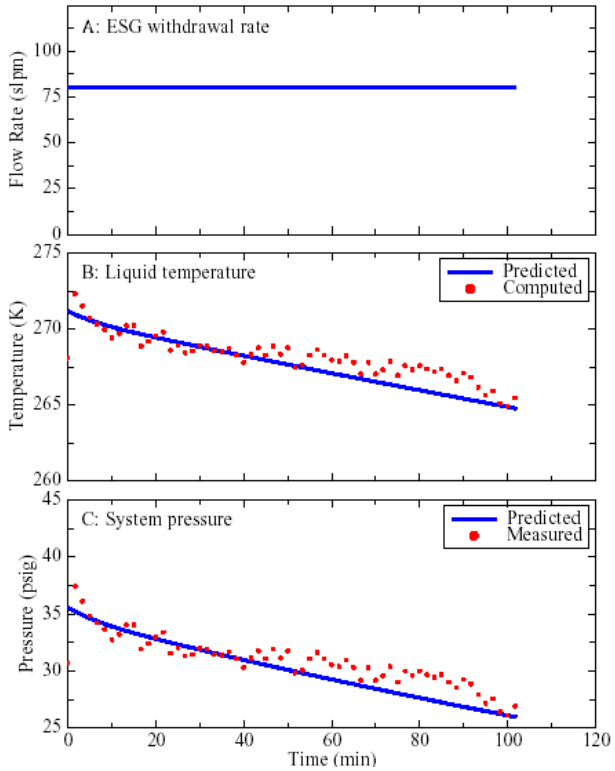

Figure 12. Comparison of model predictions with the experimental data for Cl_2 from a nearly half-full ton vessel with a initial charge of 460 kg.

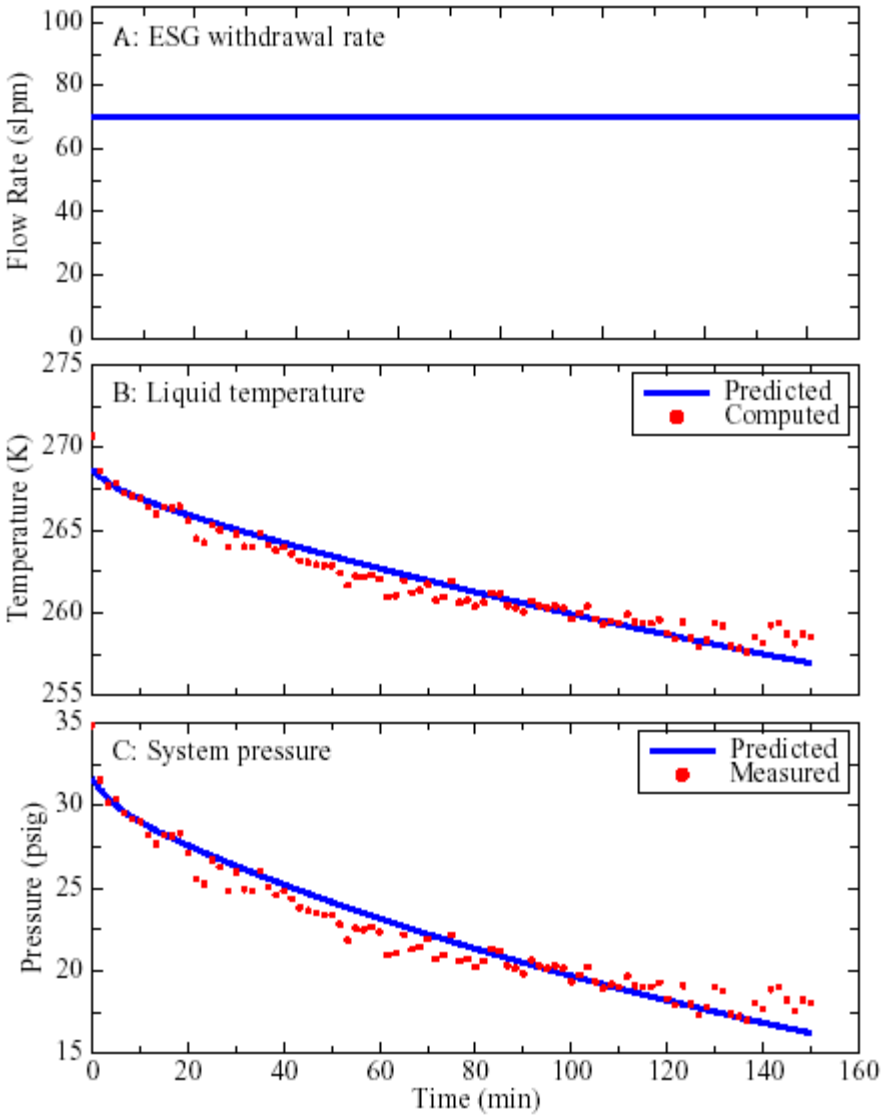

Figure 13. Comparison of model predictions with the experimental data for Cl_2 from a nearly empty ton vessel with a initial charge of 200 kg.